Mycobacteria

RESEARCH

Open Access

Establishment of minimum protein standards for *Mycobacterium tuberculosis*-derived extracellular vesicles through comparison of EV enrichment methods

Joan M. Ryan[1,3†], Kimberly Shelton[1†], Monika Dzieciatkowska[2], Nicole Kruh-Garcia[1,4] and Karen M. Dobos[1*]

Abstract

Mycobacterium tuberculosis extracellular vesicles (MEV) have been described as having potent immunological activities that are both beneficial and harmful to the host. Key to understanding this conflicting information is the proteomic characterization of MEVs. However, there is neither a standard for a purification method nor markers to assess relative purity and quality of MEVs. In this study, we purified MEVs by four different methods (simple ultracentrifugation, differential density gradient-based ultracentrifugation, qEV size exclusion chromatography, and Capto™Core size exclusion chromatography) and assessed the variability of MEV characteristics (size, concentration, appearance, purity, and protein content) amongst isolation methods. The vesicle appearance and size were consistent across all methods; however variability was found between and within all methods, with simple ultracentrifugation demonstrating the most variability both in reproducibility and purity. Protein concentration and content, and particle yield and purity, varied amongst all methods. The two size exclusion chromatography-based methods were more technically reproducible than either ultracentrifugation-based method, while qEV size exclusion chromatography and differential density gradient ultracentrifugation afforded MEV samples of the highest purity. Nonetheless, all methods had 7 proteins in common, the Sec-independent membrane bound twin-arginine translocase TatA (Rv2094c), the periplasmic phosphate-binding lipoprotein PstS3 (Rv0928), the heparin binding hemagglutinin HBHA (Rv0475), lipoprotein antigens LprG (Rv1411c) and LpqH (Rv3763), a member of the conserved 13E12 repeat protein family P95201 (Rv0393), and the tuberculin related peptide Rv0431 (P96277), suggesting the use of these proteins as qualitative markers of MEVs versus contaminants, in addition to size and appearance criteria, to benefit reproducibility and consensus for ongoing MEV studies.

Keywords *Mycobacterium tuberculosis*, Extracellular vesicles, Enrichment, Mass spectrometry

† Joan M. Ryan and Kimberly Shelton contributed equally to this work.

*Correspondence:
Karen M. Dobos
Kdobos@colostate.edu
Full list of author information is available at the end of the article

Background

Tuberculosis (TB), caused by *Mycobacterium tuberculosis*, is one of the oldest diseases known to affect humankind [1]. It has been over 140 years since the *M. tuberculosis* bacillus was first described, yet TB remains a public health crisis. It is one of the leading causes of death overall in low- and lower-middle-income countries, and it is one of the leading causes of death due to an infectious agent world-wide [2, 3]. TB can have both pulmonary and extrapulmonary manifestations, and those infected with *M. tuberculosis* can present a range of symptoms or can even be asymptomatic [4–13]. The varying spectrum of TB disease contributes to the difficulty in public health measures to eradicate it, with nearly a quarter of the world population harboring the bacteria [2].

In addition to the varied presentations of TB disease, the host–pathogen interaction that occurs during *M. tuberculosis* infection is complex. Improving our understanding of this dynamic interaction contributes to research in diagnostic, treatment, and prevention strategies. One way *M. tuberculosis* interacts with the host is through the active secretion of proteins and other macromolecules. The culture filtrate proteins (CFP) of *M. tuberculosis* have been studied for decades to better understand bacterial physiology and pathogen-host interactions. They are of particular interest for their antigenic properties, which can make them candidates for use in subunit vaccines [14–18]. *M. tuberculosis* additionally secretes several vesicular products, including multimeric proteins, glycosylated lipids, lipoglycan aggregates, and bona-fide extracellular vesicles (EVs) [19–25].

The mechanisms of mycobacterial EV biogenesis and the contents and functions of *M. tuberculosis* EVs (MEVs) are ongoing areas of investigation [24]. However, experimental variation in mycobacterial EV literature has complicated a thorough understanding of EV biogenesis, content, and function. The impact of the EV separation technique on the composition and function of the resulting preparation has been documented for a variety of systems, from human biofluids and eukaryotic cell culture to helminth and bacterial cell culture [26–29]. Parameters within purification methods, such as centrifugation settings, also significantly impact the resulting EV material [30]. In addition, EVs are released from cells into a complex matrix of various biomolecules. Therefore, when performing in vitro studies, the growth phase and media conditions from which EVs are collected can impact the types of molecules present and the volume of EVs obtained [25, 27, 28, 31–36].

A variety of EV enrichment and separation techniques have been used across MEV studies, such as ultracentrifugation, density gradient ultracentrifugation, and size exclusion chromatography, each of which has its own advantages and disadvantages (Table 1).

Density gradient ultracentrifugation was one of the first methods for separating EVs and is used for MEV enrichment [4, 16, 21, 22, 25, 29, 37–42]. A handful of publications have employed alternative workflows including ultracentrifugation alone [20, 43–45] or size exclusion chromatography (SEC) [29, 37, 46, 47]. A thorough comparison of these methods specific to MEV preparations has not been performed; such studies have been conducted to establish quality criteria for other EV preparations [26, 28, 29, 48]. Therefore, in this study, we used

Table 1 Advantages and disadvantages of mycobacterial EV (MEV) preparation methods

Technique	Advantages	Disadvantages
Ultracentrifugation	• Straightforward process • Inexpensive after centrifuge purchase • Widely used	• Instrument dependent • Low separation efficiency • Vesicle aggregation/potential damage or lysis • Published methods often lack details about instrumentation, rotors, and conditions
Density Gradient Ultracentrifugation	• High separation efficiency • Inexpensive after centrifuge purchase • Widely used • Additional dimension of separation by density vs size only	• Time consuming • Instrument dependent • Complex process • Low yield • Vesicle aggregation • Gradient medium removal required prior to analysis • Published methods often lack details about instrumentation, rotors, and conditions
Size Exclusion Chromatography	• High separation efficiency • Scalable • Straightforward process • Automation capable • Preserves EV integrity • Gentle	• Reagent and consumables cost • Dilute output • Can be challenging to define desired fractions based on overlap of EV markers and contaminants

our established culture condition for the harvest of culture filtrate proteins [49] to explore the sole effect of four different enrichment methods (ultracentrifugation, density gradient ultracentrifugation, Capto™Core SEC, and qEV SEC) on MEV size, appearance, yield, purity, protein composition, and method reproducibility. We found no significant differences in MEV size or appearance between methods. However, the two size exclusion methods, Capto™Core and qEV, were more reproducible across replicates, and higher MEV purity was achieved when density gradient or qEV separation was performed. Additionally, seven proteins (TatA, PstS3, HBHA, LprG, LpqH, P95201, and P96277) were identified in all MEV samples, regardless of the method used to enrich for MEVs. We propose that these proteins be used as standards, in addition to traditional size and appearance criteria, to ensure the quality of studies using MEVs.

Methods

M. tuberculosis culture and culture filtrate protein generation

All procedures involving live, virulent *M. tuberculosis* were performed in a biosafety level 3 laboratory (BSL- 3) at Colorado State University. These cultivation and CFP generation methods were adapted from previously published methods [47, 49].

Briefly, *M. tuberculosis* strain H37Rv was plated using 200 µL of frozen glycerol stock on 7H11 +10% OADC agar plates (15 ×150 mm). After four weeks of growth at 37 °C, the bacterial lawn from each plate was collected, cells were transferred to a Fernbach flask containing 900 mL Glycerol-Alanine-Salts (GAS; [50]) medium, and samples were cultured at 37 °C until mid-log phase. Three Fernbach flasks were used to inoculate forty 350 mL roller bottles containing GAS media, and samples cultured at 37 °C for 14 days. Samples were harvested at late-log phase growth, with optical densities ranging between OD_{600} of 6.0–8.0. Three separate harvests, each of forty roller bottles, were used for this study.

Culture filtrate was separated from bacterial cells by 0.2 µm filtration with a VacuCap 90 vacuum filtration device (Pall Corporation). Sterile filtrate was removed from BSL- 3 for further processing at BSL- 2. The filtrate was concentrated 40-fold by ultrafiltration using a 5 kDa MWCO filter (Millipore Sigma). Buffer exchange into 10 mM ammonium bicarbonate was subsequently performed by ultrafiltration, and the concentrated sample was filtered through a 0.2 µm PES filter. Total protein was determined using the bicinchoninic acid assay (BCA) (Pierce™ Thermo Scientific). The resultant culture filtrate protein (CFP) was qualified by silver stain and western blots for the presence of DnaK (Rv0350), PstS1 (Rv0934), GroES (Rv3418c), Ag85 complex (Rv3804c, Rv1866c, Rv0129c), and SodA (Rv3846). GroEL2 (Rv0440), a cell lysis marker, was used as a negative control in western blots to ensure that autolysis of the bacilli was not present at sample harvest. The following reagents used here were obtained through BEI Resources, NIAID, NIH: Monoclonal Anti-*Mycobacterium tuberculosis* DnaK (Gene Rv0350), NR- 13609; PstS1 (Gene Rv0934), NR-13790; GroES (Gene Rv3418c), NR- 13824; Ag85 complex (Genes Rv3804c, Rv1866c, Rv0129c), NR- 13816; SodA (Gene Rv3846), NR- 13810; GroEL2 (Gene Rv0440), NR-13813. Each batch of CFP was stored at 4 °C prior to use.

M. tuberculosis (MEV) enrichment

CFP ultrafiltration

Ultrafiltration was performed using a 100 kDa MWCO Centricon Plus − 70 centrifugal filter (Millipore Sigma). The filter was prepared by adding 25 mL phosphate-buffered saline without calcium or magnesium (PBS) to the top of the unit followed by centrifugation for 10 min at 2,800 ×g, 4 °C. Residual PBS was discarded from the unit. CFP was added to the top of the filter unit (up to 60 mL at a time) and centrifuged in 10 min increments at 2,800 ×g at 4 °C. The first 50 mL of 100 kDa CFP flow through (100 FT) was saved at 4 °C for downstream analysis. Once all the CFP was reduced to the filter's volume, 60 mL PBS was added to the unit and concentrated for 5 washes. One milliliter of PBS was added to each filter column directly followed by 3 mL PBS in the top of the unit. The filter was inverted into the collection cup for a recovery spin at 57 ×g for 5 min at 4 °C. An additional 1 mL of PBS was added to each filter and allowed to sit while the retentate was transferred out of the recovery cup. A second recovery spin was performed, and that retentate was pooled with the first for a total of approximately 7 mL retentate. The 100 kDa retentate (100R) was passed through a 0.8 µm/0.2 µm dual PES filter (Pall Corporation) using a 10 mL syringe. The total protein for the 100R and 100 FT was determined by BCA. The filtered 100 kDa CFP retentate was stored at 4 °C prior to use.

Capto™Core size exclusion chromatography

Capto™Core 700 (GE Healthcare Life Sciences) resin was packed into Poly-Prep® Columns (Bio-Rad) by adding 0.5 mL Capto™Core slurry followed by 5 mL PBS to remove the resin storage solution. The PBS wash of the slurry was performed by gravity-flow. The column was then capped at the bottom and 3 mg 100R in 5 mL PBS was gently added to the top of the column. The slurry was allowed to settle for 5 min before the cap was removed and the flow through recovered in a clean tube. After collection, the column was re-capped and the flow through was added for a second pass over the resin. The resin was allowed to settle before the cap was removed and the final flow

through recovered in a clean tube. The resin was washed twice with 0.5 mL PBS to maximize recovery, which was collected with the final flow through. Sample concentration was performed using a 4 mL 3 kDa MWCO Amicon Ultra centrifugal filter (Millipore Sigma). Capto™Core enriched MEVs (CC-MEVs) were added to the filter unit and reduced to approximately 200 µL. The concentrated CC-MEVs were transferred to a new tube, and the filter was rinsed twice with 200 µL PBS. The wash material was pooled with the concentrated CC-MEVs, and the final volume was recorded. For each batch of 100R, the three technical replicates were normalized by volume with the addition of PBS.

qEV size exclusion chromatography

Izon qEV original 35 nm columns, containing Sepharose CL- 2B were used with an automatic fraction collector (AFC) following the manufacturer recommendations (Izon Science Limited). After equilibrating to room temperature, the qEV column was installed on the AFC and flushed with 60 mL PBS. The AFC was programmed to collect 20 ×500 µL fractions. Three mg of 100R brought to 0.5 mL with PBS was applied to the top of the column. Once the sample had run into the column, 15 mL PBS was added to the top of the column. The AFC collected fractions after the column void volume had flowed through. All fractions were tested for their protein content by BCA and EV concentration by nanoparticle analysis. The first three fractions collected reproducibly contained the qEV-enriched MEVs (qEV-MEVs), as evidenced by the concentration (1×10^9 vesicles/ml in fractions 1 and 2, and $3 \times 10^8 - 1 \times 10^9$ vesicles/ml in fraction 3) and MEV size (94–120 nm). Fractions 4–12 contained a sequentially decreased concentration of vesicles to 1 10^5 MEVs/ml and MEVs were undetectable in later fractions. Fractions 1–3 were pooled together. After collection was complete, the qEV column was cleaned with 0.5 mL of 0.5 M NaOH followed by 60 mL PBS. Once all three replicates had been run, the column was stored in 0.05% NaN_3 at 4 °C. One column was used per 100R batch to avoid lot-to-lot cross-contamination.

Ultracentrifugation

Centrifuge rotor buckets for a SW 32.1 Ti swinging bucket rotor (Beckman Colter) were cooled to 4 °C. Thinwall polypropylene tubes 16 ×96 mm (Beckman Coulter) were rinsed with 70% ethanol and allowed to air dry. Tubes were filled with 16 mL PBS followed by the addition of 3 mg 100R. Samples were centrifuged at 100,000 ×g for 1 h at 4 °C. The supernatant was decanted from the invisible pellets by pouring smoothly and swiftly in one motion away from the expected pellet location. The pellets were each resuspended in 500 µL PBS and transferred to a new tube.

OptiPrep™ density gradient separation

The same ultracentrifuge, rotor, and tubes described above were used for density gradient ultracentrifugation. Ultracentrifuge-concentrated MEVs (UC-MEVs) were transferred to a new, dry polypropylene tube 16 ×96 mm (Beckman Coulter) and mixed with 1.5 mL OptiPrep™ density gradient medium (Millipore Sigma) to achieve a 45% iodixanol solution. Subsequently, 1.5 mL layers of 40–5% OptiPrep™ in PBS in decreasing increments of 5% were gently overlaid on the sample followed by 2 mL PBS. Samples were centrifuged at 100,000 ×g for 16 h at 4 °C. Fractions were collected with a 1 mL pipette starting from the top of each gradient and transferred to new tubes. Fractions 8–12, which contained the MEVs, were pooled. Buffer exchange to PBS was performed with a 100 kDa MWCO Amicon filter (Millipore Sigma) and centrifugation for 10 min at 2,800 ×g, 4 °C. Residual PBS was discarded from the unit. The filter was refilled with PBS, and the sample was filtered five additional times to ensure removal of residual iodixanol. The concentrated density-gradient-enriched MEVs (DG-MEVs) were transferred to a new tube, and the filter was rinsed twice with 200 µL PBS. The wash material was pooled with the concentrated DG-MEVs, and the final volume was recorded.

All enrichment techniques were performed in triplicate on three different batches of 100R for method comparison. The total protein for each enriched sample was determined by microBCA (Pierce™ Thermo Scientific) following the manufacturer's recommendations. All MEV preparations were stored at 4 °C when not in use.

MEV analysis

Nanoparticle tracking analysis (NTA)

The concentration and size distribution of the enriched MEVs were evaluated by NTA using the NanoSight NS300 (Malvern Panalytical) with an automatic syringe pump and software version 3.4. MEV samples were diluted in PBS such that the final concentration was in the range of 10^7–10^9 particles per mL, per manufacturer/instrument recommendations. The screen gain was set to 13.1, the camera level 13, and the syringe pump to infuse at 10. The focus was adjusted as needed for each sample. Three, 30-s videos were captured for each sample. Analysis settings included a screen gain of 10 and a detection level of 5 and reported average values from the three videos. Final sample particle concentration was calculated based on the NTA results and the volume of sample diluted for measurement.

Silver stain and western blot analyses

Samples normalized by either total protein or NTA particle count were resolved by SDS-PAGE using NuPAGE Novex 4–12% Bis–Tris Gels (Life Technologies) and NuPAGE MES SDS Running Buffer (Life Technologies).

Gels were either stained with silver and imaged or transferred to nitrocellulose for western blots. Western blot membranes were blocked with 2% bovine serum albumin in TBS-T for 1 h at room temperature or overnight at 4 °C. Antibodies to GlcB (Rv1837c), LpqH (Rv3763), GroES (Rv3418c), lipoarabinomannan (LAM) (obtained through BEI Resources, NIAID, NIH: Monoclonal Anti-*Mycobacterium tuberculosis* GroES (Gene Rv3418c), NR- 13824; LpqH (Gene Rv3763), NR- 13606; GlcB (Gene Rv1837c), NR- 13799; LAM, NR- 13811) or SodC (Rv0432) [51] polyclonal) were used to probe the membranes and their target proteins detected after 1 h at room temperature or overnight at 4 °C incubation with alkaline-phosphatase conjugated secondary antibody and development (NBT/BCIP ready to use tablet, Roche, dissolved in 10 mL water). Developed membranes were air-dried and imaged.

Transmission electron microscopy (TEM)

Vesicle samples were fixed by adding an equal volume of 4% TEM grade paraformaldehyde, final concentration of 2%, then stored at 4 °C for a minimum of 24 h. Formvar/carbon-coated grids (Electron Microscopy Science) were glow discharged for 30 s before 10 µL of fixed EV sample was dropped onto the grid and allowed to sit for 5 min. Excess liquid was blotted away with filter paper. The grid was washed by floating on a 50 µL drop of ultrapure water for 30 s. Excess water was blotted away then the grid was stained by floating on a 50 µL drop of 2% uranyl acetate for 2 min. Excess stain was blotted away and the grid air dried. Grids were imaged on a JOEL JEM- 2100 F transmission electron microscope at 200 kV with spot size 5 and alpha 2.

Mass spectrometry

Twenty micrograms (protein) of each vesicle sample were resolved by SDS-PAGE, and the gels were stained with SimplyBlue SafeStain (Invitrogen). Individual sample lanes were excised from the gel and cut into approximately 1 mm^3 pieces, transferred to 1.6 mL centrifuge tubes, and destained by addition of de-stain solution (60% acetonitrile (ACN) in 0.2 M ammonium bicarbonate) and incubation at 37 °C for 30 min. This process was repeated until the gel pieces appeared to be completely de-stained. Gel pieces were dried and digest solution (Sequencing grade trypsin in 0.2 M ammonium bicarbonate at 12 µL solution per 1 µg trypsin) was added directly to the gel pieces at a ratio of 1:20 (trypsin: protein). Ammonium bicarbonate (0.2 M) was added once the digest solution was absorbed by the gel pieces, and samples were incubated at 37 °C for 16 h. Tryptic peptides were extracted by two sequential incubations at 37 °C in extraction solution (60% ACN, 0.1% trifluoroacetic acid in water). The supernatant was dried, resuspended in 20 µL of MS Buffer A (3% ACN and 0.1% formic acid in water) and peptides quantitated using a NanoDrop UV–Vis spectrophotometer, A205. The samples were stored at –20 °C until liquid chromatography-mass spectrometry/mass spectrometry (LC–MS/MS) analysis.

Samples were resolved by LC–MS/MS on a Bruker timsTOF Pro mass spectrometer coupled to an LC system (Evosep One). An aliquot of each sample was loaded onto individual Evotips for desalting and washing. Peptides were separated on a Pepsep column (15 cm, 150 µm inter-diameter), packed with ReproSil C18, 1.9 µm, 120 Å resin, using a pre-set 30 samples per day gradient on the Evosep One system (Evosep, Odense, Denmark). The Evosep system was coupled to the timsTOF Pro mass spectrometer (Bruker Daltonics, Bremen, Germany) via the nano-electrospray ion source (Captive Spray, Bruker Daltonics). The mass spectrometer was operated in PASEF mode. The ramp time was set to 100 ms and 10 PASEF MS/MS scans per topN acquisition cycle were acquired. MS and MS/MS spectra were recorded from *m/z* 100 to 1700. The ion mobility was scanned from 0.7 to 1.50 Vs/cm^2. Precursors for data-dependent acquisition (DDA) were isolated within ± 1 Th and fragmented with an ion mobility-dependent collision energy, which was linearly increased from 20 to 59 eV in positive mode. Low-abundance precursor ions with an intensity above a threshold of 500 counts but below a target value of 20,000 counts were repeatedly scheduled and otherwise dynamically excluded for 0.4 min.

Data analysis

Western blot image analysis

Western blot images were converted to grayscale for analysis in ImageJ (version 1.53) [52]. The largest band of interest on the blot was used for setting the region of interest (ROI) size for analysis. Measurement for each band was performed using the mean gray value of the ROI. Background values were also generated by selecting three random areas as the ROI. All values were inverted by subtracting the pixel density recorded by Image J from 255, the maximum pixel value. The background was then subtracted to obtain the final intensity value for the relative quantification of band intensity.

Mass spectrometry data processing and analysis

Database searches were performed on raw MS data files (in the.d Bruker format) using FragPipe (version 21.1) on

a Windows 10 system with Java (11.0.9.1), equipped with MSFragger (version 4.0), IonQuant (version 1.10.12), Philosopher (version 5.1.0), and Python (version 3.9.13) [53–59]. Mass spectra were searched using MSFragger and an LFQ-MBR workflow for IM-MS data against an *M. tuberculosis* H37Rv database (UniProt, downloaded March 22, 2024; 8,226 entries with decoys (50%; 4,113 entries) and common contaminants added). MSFragger parameters for the search included a precursor mass tolerance of −20 to 20 ppm and a fragment mass tolerance of 20 ppm, with 'Mass calibration, parameter optimization' selected and isotope error of 0/1/2/3, with enzymatic (trypsin) cleavage, with cuts at KR and no cuts at P and one missed cleavage allowed. Peptide length was set at 10–50 and peptide mass range at 900–5,000. Oxidized methionine (mass delta of 15.9949) and cysteine carbamidomethylation (mass delta of 57.02146) were included as variable modifications, each with a maximum of 3 occurrences. Under 'Advanced Options' of MSFragger, the default options were used. Validation tools were used, including PSM validation and Percolator (min probability set to 0.8; with command line options: –only-psms –no-terminate –post-processing-tdc; options to predict RT and predict spectra under 'Rescoring Using Deep Learning Prediction' tab were also selected) along with ProteinProphet (with command line options: –maxppmdiff2000000). The option to generate reports was selected, with filter (–sequential –prot 0.01), and the options to generate MSstats files, remove contaminants, generate peptide-level summary, and generate protein-level summary were selected. MS1 quant was also run with IonQuant, using the loaded Quant defaults.

Statistical analysis

RStudio (2021.09.0 Build 351) using R for statistical computing (version 4.1.1) was used to generate graphs and plots [60]. All coding for statistical analyses performed in RStudio is provided in the Supplementary Material. Prior to statistical tests for differences among means, samples were evaluated for normality by histogram, QQ Plot, and Shapiro–Wilk's test (Supplementary Material Figure S2). If normality was met, equal variance was determined by Bartlett's test. If normality and equal variance assumptions were met, ANOVA with post-hoc Tukey or Student's t-test was used. If either assumption was violated (p-value < 0.05), the nonparametric Kruskal–Wallis test followed by pairwise Wilcoxon signed-rank test was performed. For the proteomics mass spectrometry data analysis, which occurred later, RStudio (2023.06.1 Build 524) using R for statistical computing (version 4.2.2) on a Windows 10 system was used to generate graphs and plots and perform statistical analyses [60–76]. The code for this can also be found in the Supplementary Material. For analyzing the mass spectrometry data, the MaxLFQ intensity (normalized peptide intensities according to the MaxLFQ method) values [77] for all samples for the proteins of interest (see Results section) were extracted from the entire output (the 'combined_protein.csv' file) provided by Fragpipe from the database search described above. Then, as above, normality for the MaxLFQ intensity for each protein of interest was evaluated by histogram, QQ plot, and Shapiro–Wilk's test (Supplementary Material Figure S3). Normality was not met for any of the data tested, and therefore the nonparametric Kruskal–Wallis test and nonparametric pairwise Dunn's test (with the Bonferroni method) were performed to evaluate statistical differences among the samples for each protein of interest.

Results

EV morphology and size

Visualization of formaldehyde-fixed MEVs from each method by TEM revealed that regardless of the method, all samples include MEVs of anticipated sizes and morphologies (Fig. 1). Some of the variation in vesicle shape is artifactual and can be attributed to the drying process for TEM grid preparation. In addition, each method resulted in MEVs of similar size, most of which fall within a range of 95–110 nm (Fig. 2). ANOVA testing demonstrated that NTA sizes show no significant difference across the means ($p = 0.1$).

Purity and reproducibility of EV enrichment across all methods

In contrast to TEM and NTA results which indicate the MEVs enriched by each method are relatively similar in terms of size and morphology, protein recovery for MEVs enriched by each method varied. Protein recovery is significantly higher for CC-MEVs than for vesicles obtained through the other methods (Fig. 3 and Table S1). UC-MEVs have a significantly higher protein recovery than qEV-MEVs and DG-MEVs, while qEV-MEVs have a significantly higher recovery than DG-MEVs (Fig. 3). Consistent with total protein recovery, CC-MEVs also have the highest particle recovery, but the statistical significance between CC-MEVs and qEV-MEVs is no longer present (Fig. 4 and Table S2). There are significantly more particles recovered by qEV than DG, and by UC than DG, but there is no apparent difference between qEV and UC.

Technical and biological replication analyses were also performed. Technical replicates demonstrated acceptable coefficients of variation (CoV), 11.55, 15.39, and 13.94 for CC, qEV, and DG methods, respectively; versus the CoV for the UC enrichment method of 28.18 (Table 2). Replicability was challenged for both ultracentrifugation methods when the biological replicate CoV was

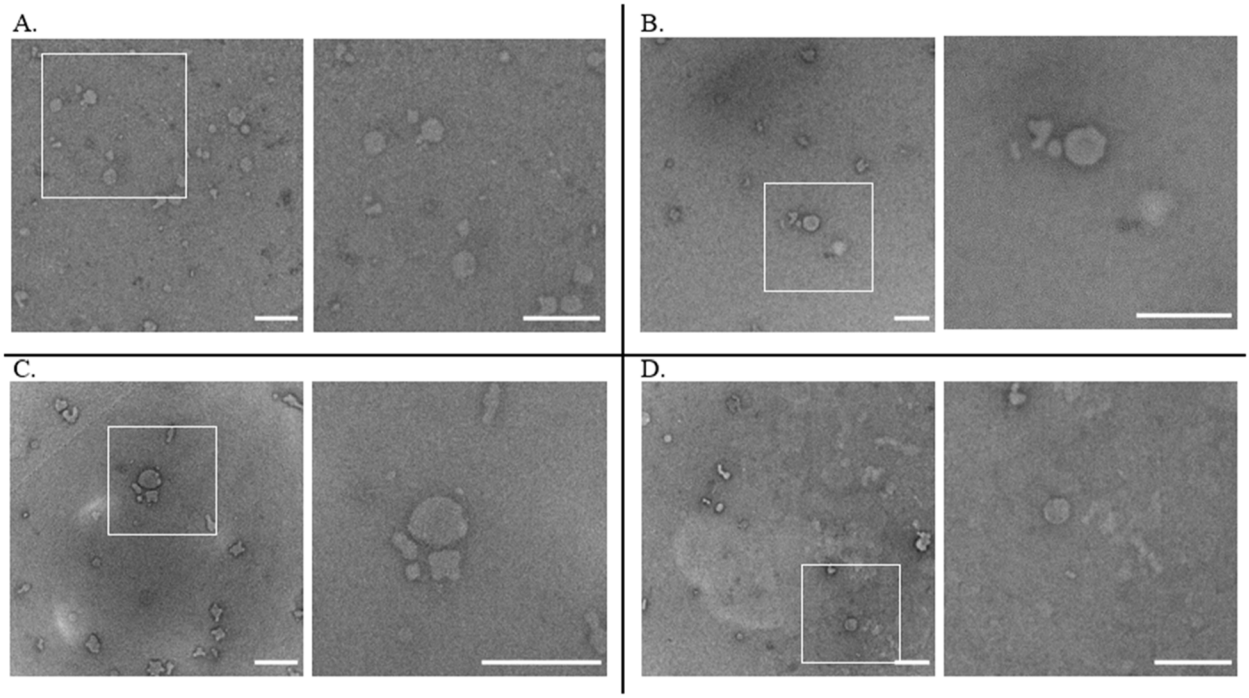

Fig. 1 Representative TEM images by enrichment method reveal vesicles of varying sizes and morphologies. Representative TEM images are shown for vesicles obtained through the (**A**) Capto™Core, (**B**) Density Gradient, (**C**) qEV, and (**D**) Ultracentrifugation methods. For each method, the image on the right is a zoomed-in view of the white box present in the image on the left. Scale bars represent 200 nm. A representative TEM of PBS buffer and MEV excluded culture filtrate proteins is provided as supplementary data, Figure S1. (Images adapted from Ryan, Joan M. Enrichment and separation of Mycobacterium tuberculosis extracellular vesicles with a side of biosafety and biosecurity. Ph.D. diss., Colorado State University, 2022. Fort Collins, CO, USA. ProQuest ID 29065918

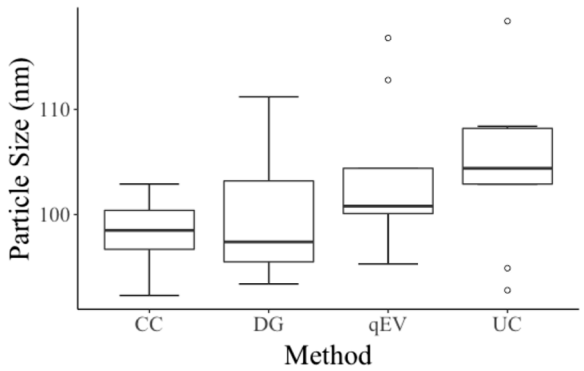

Fig. 2 Box plots of mean particle size by NTA reveal that vesicles obtained by each method fall within a similar size range. There was not sufficient evidence to indicate a significant difference among the means ($p = 0.1$ by ANOVA)

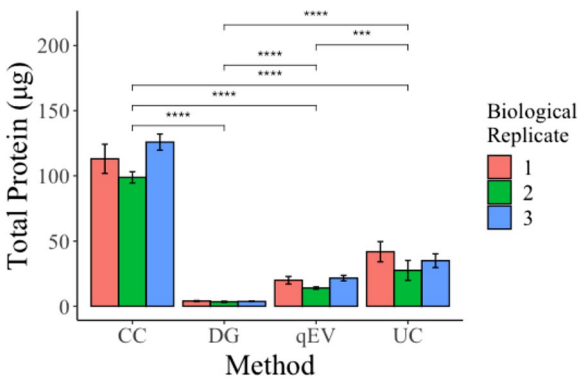

Fig. 3 Comparing protein recovery reveals that there were differences in the amount of total protein recovered across the various MEV enrichment methods. The total protein recovered is charted by method and color-coded by biological replicate. CC-MEVs appeared to have the highest protein recovery. The error bars represent the standard deviation of the technical replicates within the biological replicate. Significance from pairwise Wilcoxon signed-rank test indicated as $p < 0.001$***, and $p < 0.0001$****

calculated, with values of 52.9 and 69.1, for UC and DG, respectively (Table 2).

Finally, analysis of the ratio of particles to protein across the methods and amongst biological replicates was performed as the final assessment of MEV purity. This analysis affirmed the low CoV calculated for technical and biological replicates of both size exclusion methods, especially CC, and similarly highlighted the challenge of replication for both ultracentrifugation

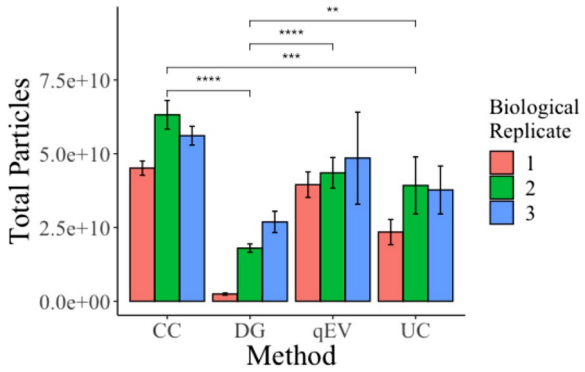

Fig. 4 Comparing total particles obtained across MEV enrichment methods reveals variation. The number of total particles recovered is charted by method and color-coded by biological replicate. Similarly to the protein recovery, there are significant differences in total particle yield across the methods. The error bars represent the standard deviation of the technical replicates within the biological replicate. Significance from Student's t-test indicated as $p < 0.01$**, $p < 0.001$***, and $p < 0.0001$****

methods, notably DG (Fig. 5). Analysis of the highest particle per protein ratios demonstrated that qEV and DG enrichment methods afforded the highest ratios, and thus greatest purity, with 2.45×10^9 and 4.45×10^9 particles per ug of protein. Interestingly, CC enrichment yielded the least pure preparation, with 0.5×10^9 (or 4.97×10^8) particles per ug of protein (Table 2 and Fig. 5).

Analysis of specific protein markers across enrichment methods

To investigate the proteomic profile of MEVs enriched by each method, samples were digested with an in-gel-based trypsin digestion protocol and analyzed by LC–MS/MS. The resulting data was processed using the database search tool, MSFragger, within the program FragPipe, against a database for the proteome of *M. tuberculosis* H37Rv. A comparison of the total number of proteins identified in this search across the MEV enrichment methods indicates that, as expected, the CFP material had the greatest number of proteins (Fig. 6). Following CFP, the 100R material and CC-MEVs had the greatest number of proteins. UC-MEVs and qEV-MEVs had a comparable number of identified proteins and DG-MEVs had the least number of proteins identified (Fig. 6).

Beyond the total number of proteins, we initially looked specifically at four proteins, LpqH, SodC, GlcB, and GroES. These proteins are predominantly represented in MEV literature, with LpqH and SodC described as MEV-associated proteins and GlcB and GroES as contaminants [21, 42, 78]. We initially compared the MaxLFQ intensity for these proteins across MEV enrichment methods. In the case of LpqH, CC-MEVs had a higher intensity than the 100R material ($p < 0.001$), DG-MEVs ($p < 0.0001$) and the UC-MEVs ($p < 0.01$) (Fig. 7A). DG-MEVs had the lowest MaxLFQ intensity for LpqH amongst all methods, also having significantly lower intensity compared to qEV-MEVs and UC-MEVs ($p < 0.0001$ and $p < 0.01$, respectively) (Fig. 7A). In terms of SodC MaxLFQ intensity, there is a difference between CC-MEVs and DG-MEVs, qEV-MEVs, and UC-MEVs ($p < 0.001$, $p < 0.01$, and $p < 0.05$, respectively), with CC-MEVs appearing to have the highest intensity for SodC. There is also a difference between DG-MEVs and both qEV-MEVs and UC-MEVs ($p < 0.05$ and $p < 0.01$, respectively), with DG-MEVs exhibiting a lower intensity for SodC (Fig. 7B).

Table 2 Particle to protein ratio coefficients of variation for each method and biological replicate

Method	Biological Replicate	Technical Replicate Average Particles per µg	Technical Replicate Standard Deviation	Technical Replicate CoV (%)	Average Technical Replicate CoV (%)	Method Average Particles per µg	Method Standard Deviation	Method CoV (%)
CC	1	4.03E + 08	6.33E + 07	15.7	11.55	4.97E + 08	1.19E + 08	24.0
CC	2	6.40E + 08	5.15E + 07	8.0				
CC	3	4.48E + 08	4.88E + 07	10.9				
qEV	1	1.98E + 09	1.62E + 08	8.2	15.39	2.45E + 09	6.32E + 08	25.8
qEV	2	3.12E + 09	2.47E + 08	7.9				
qEV	3	2.25E + 09	6.77E + 08	30.1				
UC	1	5.62E + 08	4.86E + 07	8.7	28.18	1.07E + 09	5.65E + 08	52.9
UC	2	1.53E + 09	6.56E + 08	42.9				
UC	3	1.11E + 09	3.68E + 08	33.0				
DG	1	6.21E + 08	1.06E + 08	17.1	13.94	4.43E + 09	3.07E + 09	69.1
DG	2	5.31E + 09	4.32E + 08	8.1				
DG	3	7.37E + 09	1.22E + 09	16.6				

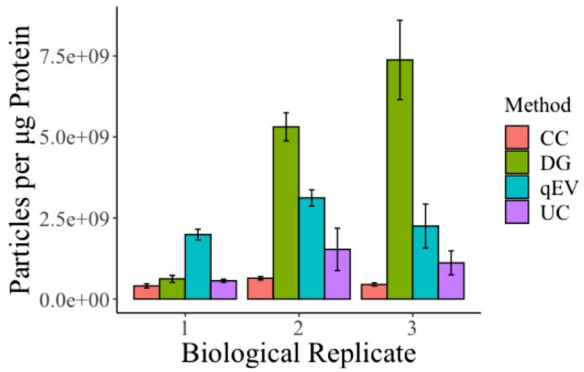

Fig. 5 Particle to protein ratio for each MEV enrichment method, grouped by biological replicate. The number of particles per µg of protein is charted by method and color-coded by biological replicate. The error bars represent the standard deviation of the technical replicates within the biological replicate

Mass spectrometry analysis reveals that MEVs obtained by all tested methods do indeed contain LpqH, although there are differences across the methods (Fig. 7A). When considering the intensity of SodC following mass spectrometry analysis, CC-MEVs appear to have the highest intensity, with qEV-MEVs and UC-MEVs appearing to be relatively similar (Fig. 7B). These findings indicate that MEVs obtained by DG generally exhibit lower levels of SodC and LpqH whereas MEVs obtained by CC exhibit higher levels of these proteins. This somewhat confounded our analysis of MEVs by particle quantity and particle purity.

The MaxLFQ intensity findings for the contaminants, GlcB and GroES, demonstrated that all MEV enrichment methods result in a lower GlcB intensity than the 100R starting material, although only the difference between 100R and DG-MEVs and between 100R and qEV-MEVs that rises to statistical significance ($p < 0.0001$ for both). There are also significant differences between CC-MEVs and both DG-MEVs and qEV-MEVs ($p < 0.001$ for both) along with differences between UC-MEVs and both DG-MEVs and qEV-MEVs ($p < 0.0001$ for both), with DG-MEVs and qEV-MEVs exhibiting lower MaxLFQ intensity for GlcB than either CC-MEVs or UC-MEVs (Fig. 8A). In the case of GroES, there are no statistically significant differences between the 100R starting material and any of the MEV enrichment methods. However, the GroES intensity for each method, apart from UC, appears to be relatively low. UC-MEVs appear to have the highest GroES intensity when compared to CC-MEVs ($p < 0.05$), DG-MEVs ($p < 0.0001$), and qEV-MEVs ($p < 0.0001$) (Fig. 8B). Taken together, these proteomic findings support that DG and qEV enrichment methods result in MEV preparations with the least protein contaminants (GlcB and GroES), and thus greatest purity.

Visualizing protein variation across enrichment methods

We performed silver staining along with western blots to validate our mass spectrometry findings. Each MEV enrichment method was probed with specific antibodies to detect the protein markers of interest (LpqH, SodC,

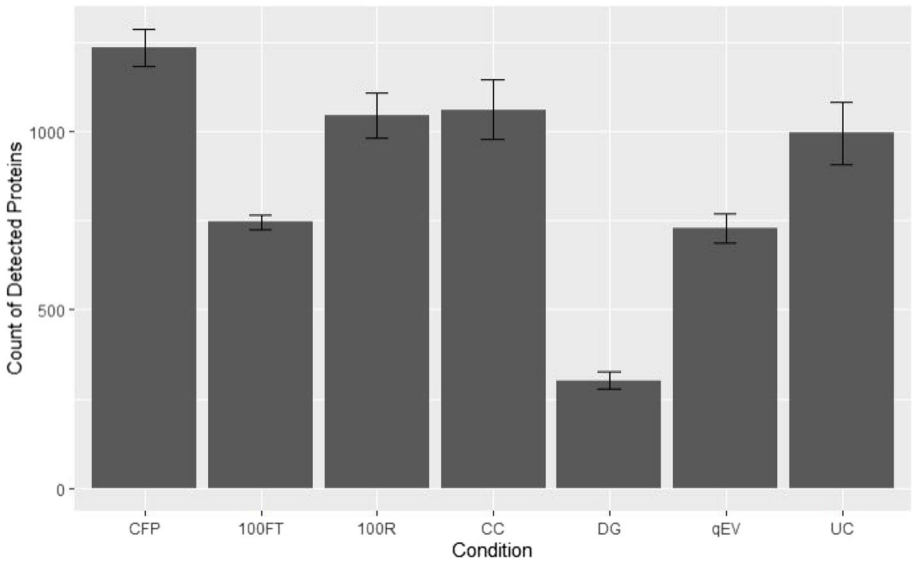

Fig. 6 Number of proteins identified through proteomics analysis followed by FragPipe analysis, across enrichment methods. Untargeted proteomic analysis by LC–MS/MS followed by analysis with a database search tool (FragPipe) revealed that the number of proteins identified across MEVs obtained from the various MEV enrichment methods varies, with DG-MEVs resulting in the fewest proteins identified. Error bars represent protein count plus and minus the standard deviation of protein count

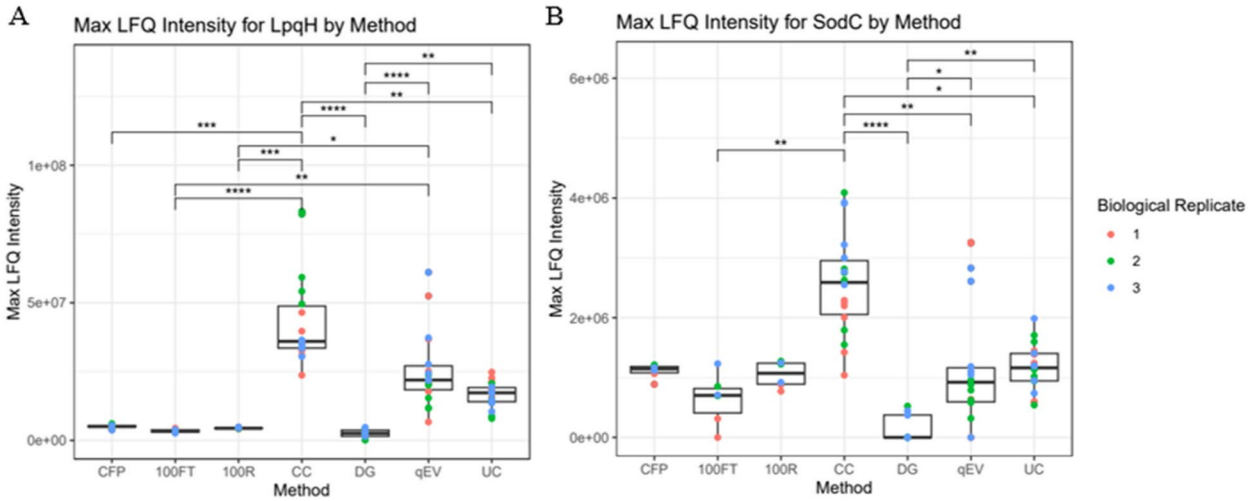

Fig. 7 MaxLFQ intensity of MEV-associated proteins across MEV enrichment methods. Analysis of MEV-associated proteins (LpqH and SodC) following mass spectrometry indicates that MEVs obtained by all methods have detectable levels of both proteins, with DG-MEVs exhibiting the lowest MaxLFQ intensity for both. Significance is indicated as $p < 0.05$*, $p < 0.01$**, $p < 0.001$***, and $p < 0.0001$****

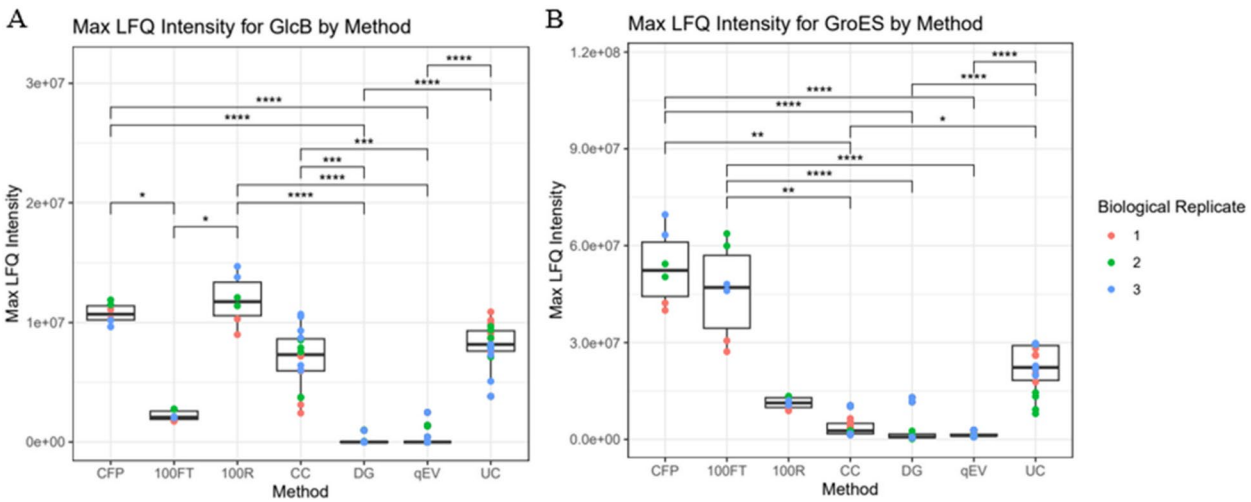

Fig. 8 MaxLFQ intensity of contaminant proteins across MEV enrichment methods. Analysis of contaminant proteins (GlcB and GroES) by mass spectrometry indicates that MEVs obtained from DG and qEV exhibit lower MaxLFQ intensities for these proteins than MEVs obtained by CC and UC. Significance is indicated as $p < 0.05$*, $p < 0.01$**, $p < 0.001$***, and $p < 0.0001$****

GlcB, GroES). Detection of LAM was added to these assays as an ancillary mycobacteria marker.The silver stain and western blot results for biological replicate 2 are shown as representative (Fig. 9). Silver stain and western blot images for biological replicates 1 (Due to inadequate recovery, biological replicate 1 for DG-MEVs was not included in analyses by silver stain or western blots) and 3 are available as supplementary material (Figure S4 and Figure S5).

LpqH is detected across all samples in western blot analysis, and further intensity analysis of the blots (Fig. 10) confirms that all the methods demonstrate LpqH enrichment (Fig. 10D) when compared to the 100R material. This aligns with our proteomics findings in which LpqH is detected in MEVs from all methods including a higher MaxLFQ intensity in all methods compared to the 100R material. Western blot analysis for SodC indicates that this protein is present in MEVs obtained from all four methods, again aligning with the proteomics mass spectrometry analysis. According to mass spectrometry analysis, the MaxLFQ intensity of SodC is lowest in DG-MEVs and appears highest in CC-MEVs, with qEV-MEVs

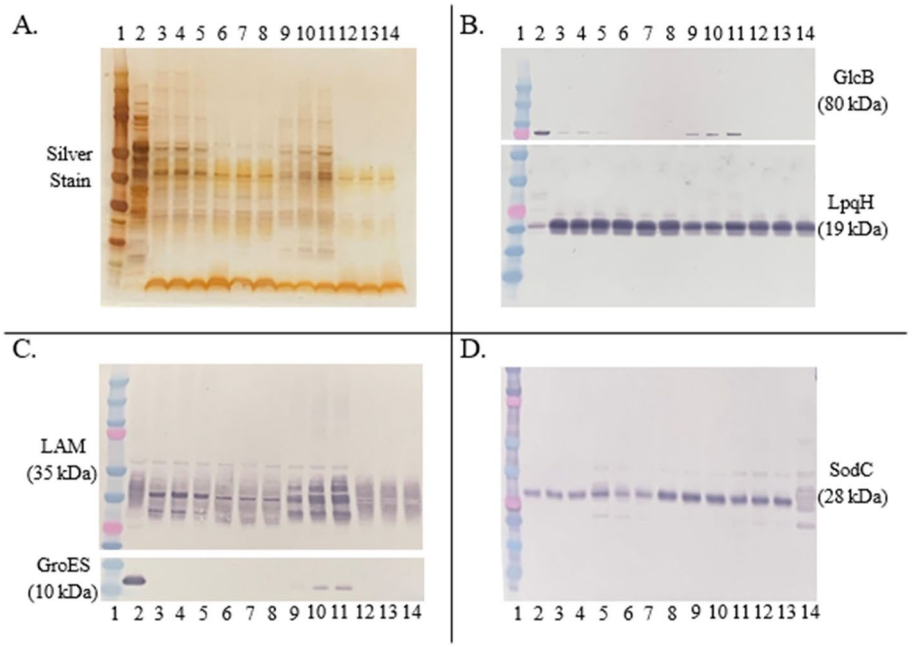

Fig. 9 Silver stain and western blots of biological replicate 2. **A** Silver stain and (**B**-**D**) Western blots for each technical replicate of biological replicate 2. All are loaded in the following format: 1 = ladder, 2 = 5 µg 100R, 3–5 = 1E9 CC-EV 2.1–2.3, 6–8 = 1E9 qEV-EV 2.1–2.3, 9–11 = 1E9 UC 2.1–2.3, and 12–14 = 1E9 DG 2.1–2.3. Image adapted from Ryan, Joan M. Enrichment and separation of Mycobacterium tuberculosis extracellular vesicles with a side of biosafety and biosecurity. Ph.D. diss., Colorado State University, 2022. Fort Collins, CO, USA. ProQuest ID 29065918

and UC-MEVs having similar levels. Similarly, western blot analysis indicates differences in the levels of SodC present across MEV samples. However, as indicated by evaluation of band intensity in western blot analysis, CC-MEVs and qEV-MEVs appear to have higher levels of SodC than DG-MEVs and UC-MEVs, although the statistical significance of these differences varies across biological replicates. While the LAM banding visual patterns vary by method (Fig. 9C), the overall signal intensity demonstrates few to no significant differences, including between 100R and MEV enrichment methods (Fig. 10C).

According to silver stain results, there appears to be a more efficient reduction in contaminant proteins in qEV-MEVs and DG-MEVs when compared to the other methods (Fig. 9A). Neither GroES nor GlcB is visible for qEV-MEVs and DG-MEVs by western blot analysis (Fig. 9 B and C). In addition, both these proteins demonstrate very low western blot band intensity (Fig. 10A and B) and low MaxLFQ intensity results in qEV-MEVs and DG-MEVs. Interestingly, GroES appears most clearly in UC-MEVs by western blot (Fig. 9C). This result also aligns with proteomic analysis in which UC-MEVs exhibit the highest GroES intensity compared to MEVs from the other three methods. GlcB also appears in UC-MEVs, along with CC-MEVs, in western blot analysis. This, too, aligns with the earlier proteomic findings in which CC-MEVs and UC-MEVs have a significantly higher MaxLFQ intensity for GlcB than either DG-MEVs or qEV-MEVs (Fig. 8A). Overall, western blot analysis, and subsequent signal intensity analysis, indicates that qEV and DG most consistently result in MEVs with the least protein contaminants (GlcB and GroES), aligning with all other analyses.

Global analysis of proteins across enrichment methods

Based on inconsistencies in LpqH and SodC detection across methods, by proteomic and western blot analysis, as well as inconsistencies using these reported proteins against our other analyses, we performed an unbiased analysis of all proteins across samples to gain a revised consensus of MEV markers. To do this, we investigated the proteins shared among DG-MEVs, CC-MEVs, UC-MEVs, and qEV-MEVs. Over 1000 proteins were identified in at least 1 of our 72 LC–MS injections, and over 650 proteins remained when a minimum combined spectra count of 100 was applied (Supplementary spreadsheet, sheet 1 and 2 respectively). Further, 89 proteins were found in all methods when a low stringency analysis of only one injection (1 of 18) per method was used to compare results (Supplementary Table). When stipulated

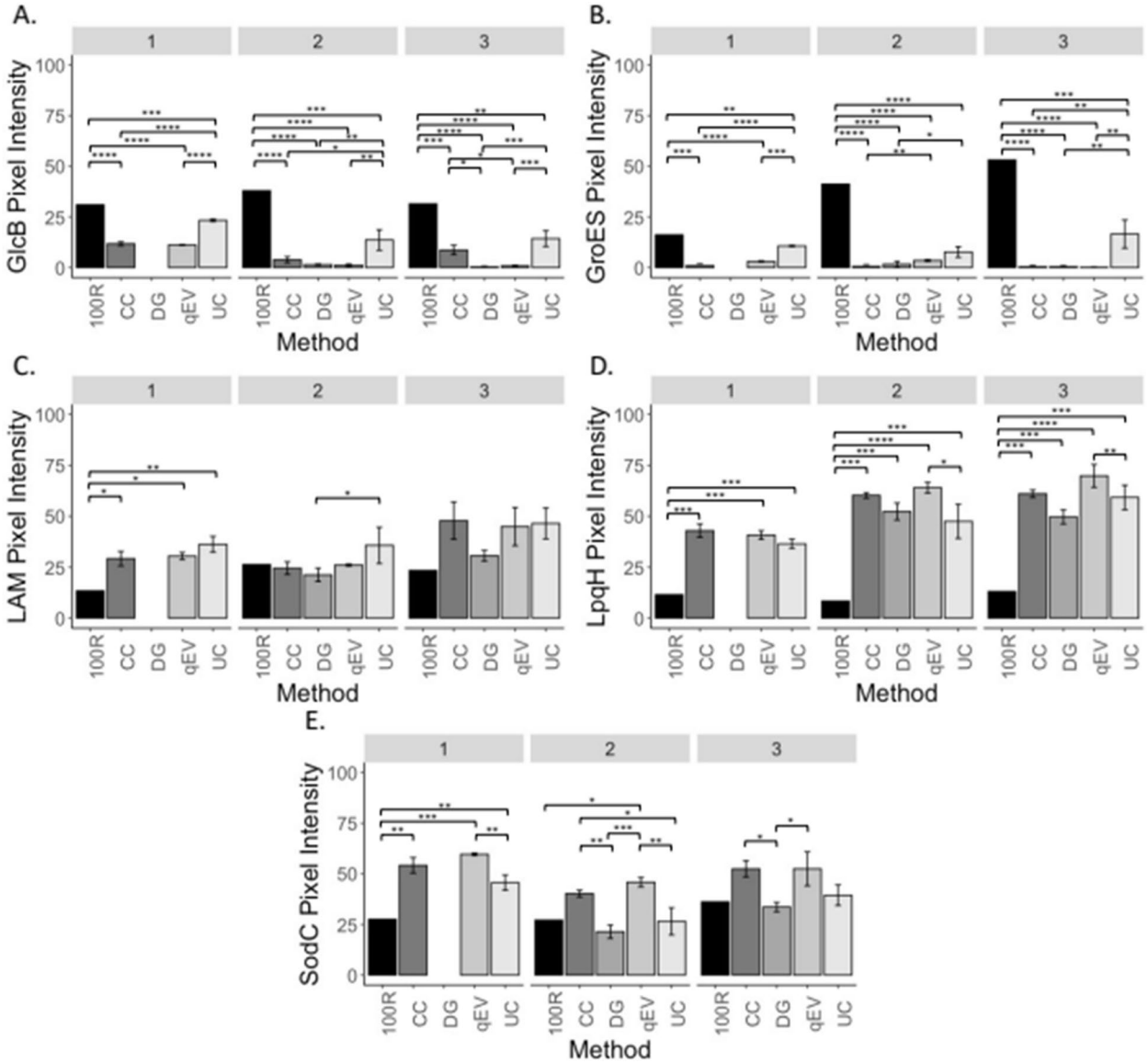

Fig. 10 Western blot intensity comparisons. Average pixel intensity for each technical replicate is shown for western blots against (**A**) GlcB, (**B**) GroES, (**C**) LAM, (**D**) LpqH, and (**E**) SodC. Each biological replicate had one western blot per antibody so a comparison among pixel intensity was performed using the Student's t-test. Significance is indicated as $p < 0.05$*, $p < 0.01$**, $p < 0.001$***, and $p < 0.0001$****

that a protein must be found in at least one-third (33%, 6 of the 18 injections) of the samples for each MEV enrichment method, we found a total of 7 proteins to be shared among MEVs obtained from all these protocols (CC, DG, qEV, UC) (Fig. 11; Table 3), with the DG method being the most discriminatory. Shared proteins across CC, qEV, and UC methods equated to 56 (Fig. 11).

LpqH is included in these common proteins and remains as an MEV proteomic standard. Four additional proteins, LprG, TatA, a sec-independent translocase protein, PstS3, a phosphate-binding protein, and HBHA, a heparin-binding hemagglutinin, were identified in all MEV enrichment methods, consistent with other studies investigating the protein content of MEVs [23]. Through this comparison of proteomics results, we also found that 199 proteins were identified in CC-MEVs that were not shared with the other groups, 189 proteins were identified in UC-MEVs that were not shared, and only one protein was identified in qEV-MEVs that was not shared with any other group. In addition, CC-, qEV-,

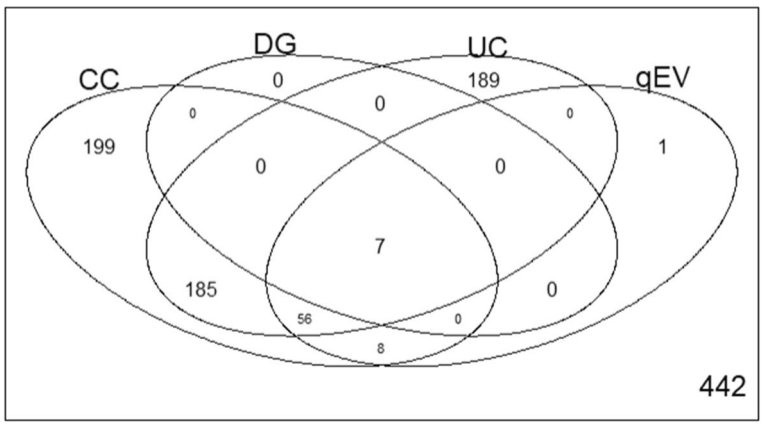

Fig. 11 Venn diagram of number of proteins shared among MEVs obtained from each protocol. With the condition that a protein must be found in at least one-third of samples within each MEV enrichment method, a Venn diagram analysis revealed 7 M. *tuberculosis* proteins to be shared among MEVs obtained using the CC, DG, UC, and qEV methods

Table 3 List of proteins shared among CC-MEVs, DG-MEVs, UC-MEVs, and qEV-MEVs

Protein	Protein Description
sp|P9 WGA1|TATA_MYCTU	Sec-independent translocase protein TatA
sp|P9 WGT7|PSTS3_MYCTU	Phosphate-binding protein PstS3
sp|P9 WIP9|HBHA_MYCTU	Heparin-binding hemagglutinin
sp|P9 WK45|LPRG_MYCTU	Lipoarabinomannan carrier protein LprG
sp|P9 WK61|LPQH_MYCTU	Lipoprotein LpqH
tr|P95201|P95201_MYCTU	Conserved 13E12 repeat family protein
tr|P96277|P96277_MYCTU	Tuberculin related peptide

and UC-MEVs appear to have similarities in their protein profiles, as they have 56 proteins in common, while CC-MEVs and UC-MEVs additionally have 185 proteins in common.

Discussion

TB is a pervasive disease in many regions of the world, and the interaction between *M. tuberculosis* and the host is complex. The release of MEVs, as one of the many ways in which the bacteria interact with the host during infection and modulate the course of disease, is of increasing interest and an area of active investigation [21, 24, 37, 43, 79]. The first report of EV production by mycobacteria was published in 2007, where scanning electron microscopy (SEM) imaging revealed vesicles associated with *M. ulcerans* biofilms. This observation led to the first purification of mycobacterial EVs and immunoprecipitation of these EVs from infected mouse tail tissues [20]. Not long after this initial publication, production of EVs by many other environmental and pathogenic mycobacterial species, including *M. tuberculosis*, was demonstrated [21, 22]. Despite these findings and ongoing investigations into MEV biogenesis, content, and function, there is currently no standardized method for obtaining MEVs or for qualifying MEV preparations.

In this study, we evaluated the impact of four different methods to obtain MEVs (UC, DG, CC, and qEV) on the characteristics of the resulting MEV preparations, including MEV size, appearance, yield, purity, protein composition, and overall method reproducibility. We found that the qEV and DG enrichment methods result in MEV preparations with the greatest purity, according to analysis of the ratio of particles to protein (Table 2 and Fig. 5) along with both mass spectrometry and western blot analysis of contaminant proteins, GlcB and GroES (Figs. 8, 9 and 10). The DG method posed most challenging for biological replicability and this should be taken into account when this method is used (Table 2 and Fig. 5). Although qEV appears to be a promising method to obtain consistent and relatively pure MEV preparations, the cost of the supplies needed for this method can be prohibitive and therefore pose a limitation to widespread use in the field.

We also identified a set of seven proteins shared among MEVs obtained from all four methods (TatA, PstS3, HBHA, LprG, LpqH, P95201, and P96277, see Table 3). Interestingly, TatA, PstS3, HBHA, LprG, LpqH, and P96277 are all associated with the cell membrane or cell wall and have been detected in association with MEVs in proteomic studies conducted by other groups [21, 23, 42]. Proteomic analysis of MEVs in previous studies demonstrated lipoprotein enrichment, with LpqH, a 19 kDa lipoprotein antigen precursor, and LprG, a conserved

lipoprotein, both of which are involved in cell wall processes, strongly represented [21, 42]. Lipoproteins made up to 10% of the identified proteins in one study [21], while they comprise only 1–2% of proteins in the whole *M. tuberculosis* genome [80]. Transmission electron microscopy (TEM) of immunogold antibody-labeled MEVs also confirmed the presence of LpqH and LprG in the membrane of MEVs [21]. These results support our finding of LpqH and LprG among the top shared proteins across MEV preparations and our proposal that these proteins be used as standards to evaluate MEV preparations. In addition, HBHA is displayed on the surface of the bacteria with a role in adhering to host cells [81]. TatA is involved in the twin-arginine translocation (Tat) protein export pathway, the components for which are located at the cytoplasmic membrane. This may explain the incorporation of TatA, and periodically TatA interacting proteins, into MEVs as they are generated and released from the surface of the bacterial cell [82]. PstS3 is a phosphate-binding lipoprotein which also serves as a ligand for host toll-like receptor 2 (TLR2) and is likewise located at the bacterial cell membrane [21, 42]. P96277 (Rv0431), a tuberculin related peptide, is enriched in the membrane fraction of *M. tuberculosis* by mass spectrometry analysis [83, 84] and was identified in previous MEV proteomics studies [42]. Interestingly, these proteins all appear to be involved in virulence, a characteristic of many of the proteins identified in other studies on MEVs [21, 42]. In fact, even the P95201 (Rv0393) protein, while its function remains unknown, has been predicted to be a virulent protein [85], which may partly explain its presence in our list of shared MEV proteins. These findings ultimately align with other MEV studies, contribute to evidence that MEVs play a role in virulence and infection, and support our proposal that these proteins be used as standards to assist in qualifying MEV preparations.

In summary, our studies demonstrate that MEV size and appearance is not affected nor different based on enrichment method. In contrast, MEV purity and the replicability of enrichment procedures for consistent MEV populations varied considerably based on the method, with qEV and DG resulting in the greatest MEV purity, yet qEV and CC having more reliable replicability compared to DG and UC. Despite these inconsistencies across preparations, all methods demonstrated a reduction in GlcB (Rv1837) as an indicator of the removal of non-MEV contaminants, and identified a set of seven proteins (TatA, PstS3, HBHA, LprG, LpqH, P95201, and P96277, see Table 3) indicative of MEV proteins. We propose using these protein standards, along with size and appearance, to qualify MEV preparations as part of continued studies on these potent contributors to immunomodulation during tuberculosis.

Supplementary Information

The online version contains supplementary material available at https://doi.org/10.1186/s44350-025-00003-8.

Supplementary Material 1

Supplementary Material 2

Supplementary Material 3.

Acknowledgements

We acknowledge Dr. Luisa Maria Nieto Ramirez for her help in brainstorming and statistical analysis ideas and Barbara Graham for providing valuable assistance with R code and data analysis and visualization for the proteomics portion of the study. We also thank Marshall Thomas for technical assistance, particularly with culture and CFP preparation. We acknowledge and thank BEI Resources, NIAID, NIH for providing antibodies for CFP analysis and western blot analyses.

Authors' contributions

J.R., K.S, and M.D Produced MEV samples, performed the assays, acquired, analyzed, and statistically validated the data. Contributed to interpretation of results: Joan M. Ryan, Kimberly Shelton, Nicole Kruh-Garcia, Karen M. Dobos J.R., K.S., and K.M.D. Wrote the main manuscripts text. J.R., K.S., N.K.G., and K.M.D. Reviewed and edited the manuscript. All Authors contributed to the conception and design of the study and reviewed the manuscript.

Funding

The research reported here was supported by the National Institute of Allergy And Infectious Diseases of the National Institutes of Health under Award Number T32 AI162691, and by award number 2016–0550 - 002 from American Type Culture Collection (ATCC) NIH NIAID Flowthrough to KMD. The content is solely the responsibility of the authors and does not necessarily represent the official views of the National Institutes of Health.

Data availability

All relevant image data are contained within this manuscript, or as supplementary materials. The mass spectrometry proteomics data have been deposited to the ProteomeXchange Consortium via the PRIDE [86] partner repository with the dataset identifier PXD056465.

Declarations

Ethics approval and consent to participate

Not applicable.

Consent for publication

Not applicable.

Competing interests

The authors declare no competing interests.

Author details

[1]Department of Microbiology, Immunology, and Pathology, Colorado State University, 2025 Campus Delivery, Fort Collins, CO, USA. [2]Biological Mass Spectrometry Facility, University of Colorado School of Medicine, Anschutz Medical Campus, Aurora, CO, USA. [3]Present Address: Office of Research Collaboration and Compliance, Colorado State University, Fort Collins, CO, USA. [4]Present Address: BioMARC, Fort Collins, CO, USA.

Received: 24 September 2024 Accepted: 30 March 2025
Published online: 15 April 2025

References

1. Daniel TM. The history of tuberculosis. Respir Med. 2006;100(11):1862–70. Available from: https://pubmed.ncbi.nlm.nih.gov/16949809/. Cited 2025 Jan 17.

2. World Health Organization. Global Tuberculosis Report 2024. 2024. https://www.who.int/teams/global-programme-on-tuberculosis-and-lung-health/tb-reports/global-tuberculosis-report-2024.
3. The top 10 causes of death. Available from: https://www.who.int/news-room/fact-sheets/detail/the-top-10-causes-of-death. Cited 2025 Jan 17.
4. Chakraborty S, Rhee KY. Tuberculosis Drug Development: History and Evolution of the Mechanism-Based Paradigm. Cold Spring Harb Perspect Med. 2015;5(8):1–11. Available from: https://pubmed.ncbi.nlm.nih.gov/25877396/. Cited 2025 Jan 17.
5. Talbot EA, Raffa BJ. Mycobacterium tuberculosis. Mol Med Microbiol. 2015;1:1637–53.
6. Martini M, Besozzi G, Barberis I. The never-ending story of the fight against tuberculosis: from Koch's bacillus to global control programs. J Prev Med Hyg. 2018;59(3):E241–7. Available from: https://pubmed.ncbi.nlm.nih.gov/30397682/. Cited 2025 Jan 17.
7. Salgame P, Geadas C, Collins L, Jones-López E, Ellner JJ. Latent tuberculosis infection - revisiting and revising concepts. Tuberculosis. 2015;95(4):373–84.
8. Dhar N, McKinney J, Manina G. Phenotypic heterogeneity in Mycobacterium tuberculosis . Microbiol Spectr. 2016;4(6). https://doi.org/10.1128/microbiolspec.TBTB2-0021-2016.
9. Moule MG, Cirillo JD. Mycobacterium tuberculosis dissemination plays a critical role in pathogenesis. Front Cell Infect Microbiol. 2020;10:65.
10. Drain PK, Bajema KL, Dowdy D, Dheda K, Naidoo K, Schumacher SG, et al. Incipient and subclinical tuberculosis: a clinical review of early stages and progression of infection. Clin Microbiol Rev. 2018;31(4):e00021.
11. Cadena AM, Fortune SM, Flynn JL. Heterogeneity in tuberculosis. Nat Rev Immunol. 2017;17(11):691–702.
12. Henry Boom W, Schaible UE, Achkar JM. The knowns and unknowns of latent Mycobacterium tuberculosis infection. J Clin Invest. 2021;131(3):e136222.
13. Baykan AH, Sayiner HS, Aydin E, Koc M, Inan I, Erturk SM. Extrapulmonary tuberculosis: an old but resurgent problem. Insights Imaging. 2022;13(1):39. Available from: http://www.ncbi.nlm.nih.gov/pubmed/35254534. Cited 2025 Jan 17.
14. The Chemical Composition of the Active Principle of Tuberculin | XV. Precipitated Purified Tuberculin Protein Suitable for the Preparation of a Standard Tuberculin1,2 | American Review of Tuberculosis. Available from: https://www.atsjournals.org/doi/abs/10.1164/art.1932.25.6.724. Cited 2025 Jan 17.
15. Målen H, Søfteland T, Wiker HG. Antigen analysis of Mycobacterium tuberculosis H37Rv culture filtrate proteins. Scand J Immunol. 2008;67(3):245–52.
16. Rodríguez-Hernández E, Quintas-Granados LI, Flores-Villalva S, Cantó-Alarcón JG, Milián-Suazo F. Application of antigenic biomarkers for Mycobacterium tuberculosis. J Zhejiang Univ Sci B. 2020;21(11):856–70.
17. Mustafa AS. Chemical and Biological Characterization of Mycobacterium tuberculosis-Specific ESAT6-like proteins and their potentials in the prevention of tuberculosis and asthma. Med Princ Pract. 2023;32(4–5):217–24.
18. Bekmurzayeva A, Sypabekova M, Kanayeva D. Tuberculosis diagnosis using immunodominant, secreted antigens of Mycobacterium tuberculosis. Tuberculosis. 2013;93(4):381–8.
19. Brown L, Wolf JM, Prados-Rosales R, Casadevall A. Through the wall: extracellular vesicles in Gram-positive bacteria, mycobacteria and fungi. Nat Rev Microbiol. 2015;13(10):620–30.
20. Marsollier L, Brodin P, Jackson M, Korduláková J, Tafelmeyer P, Carbonnelle E, et al. Impact of Mycobacterium ulcerans biofilm on transmissibility to ecological niches and Buruli ulcer pathogenesis. PLoS Pathog. 2007;3(5):0582–94.
21. Prados-Rosales R, Baena A, Martinez LR, Luque-Garcia J, Kalscheuer R, Veeraraghavan U, et al. Mycobacteria release active membrane vesicles that modulate immune responses in a TLR2-dependent manner in mice. J Clin Invest. 2011;121(4):1471–83.
22. Chiplunkar SS, Silva CA, Bermudez LE, Danelishvili L. Characterization of membrane vesicles released by Mycobacterium avium in response to environment mimicking the macrophage phagosome. Future Microbiol. 2019;14(4):293–313.
23. Palacios A, Gupta S, Rodriguez GM, Prados-Rosales R. Extracellular vesicles in the context of Mycobacterium tuberculosis infection. Mol Immunol. 2021;133:175–81.
24. Salgueiro VC, Passemar C, Vázquez-Iniesta L, Lerma L, Floto A, Prados-Rosales R. Extracellular vesicles in mycobacteria: new findings in biogenesis, host-pathogen interactions, and diagnostics. MBio. 2024;15(5):e0255223.
25. Prados-Rosales R, Weinrick BC, Piqué DG, Jacobs WR, Casadevall A, Rodriguez GM. Role for Mycobacterium tuberculosis membrane vesicles in iron acquisition. J Bacteriol. 2014;196(6):1250–6. Available from: https://pubmed.ncbi.nlm.nih.gov/24415729/. Cited 2025 Jan 17.
26. Brennan K, Martin K, FitzGerald SP, O'Sullivan J, Wu Y, Blanco A, et al. A comparison of methods for the isolation and separation of extracellular vesicles from protein and lipid particles in human serum. Sci Rep. 2020;10(1):1039.
27. Van Deun J, Mestdagh P, Sormunen R, Cocquyt V, Vermaelen K, Vandesompele J, et al. The impact of disparate isolation methods for extracellular vesicles on downstream RNA profiling. J Extracell vesicles. 2014;3(1). Available from: http://www.ncbi.nlm.nih.gov/pubmed/25317274. Cited 2025 Jan 17.
28. Davis CN, Phillips H, Tomes JJ, Swain MT, Wilkinson TJ, Brophy PM, et al. The importance of extracellular vesicle purification for downstream analysis: A comparison of differential centrifugation and size exclusion chromatography for helminth pathogens. PLoS Negl Trop Dis. 2019;13(2):e0007191.
29. Dauros Singorenko P, Chang V, Whitcombe A, Simonov D, Hong J, Phillips A, et al. Isolation of membrane vesicles from prokaryotes: a technical and biological comparison reveals heterogeneity. J Extracell vesicles. 2017;6(1):1324731. Available from: http://www.ncbi.nlm.nih.gov/pubmed/28717421. Cited 2025 Jan 17.
30. Cvjetkovic A, Lötvall J, Lässer C. The influence of rotor type and centrifugation time on the yield and purity of extracellular vesicles. J Extracell vesicles. 2014;3(1). Available from: http://www.ncbi.nlm.nih.gov/pubmed/24678386. Cited 2025 Jan 17.
31. Walker SA, Kennedy MT, Zasadzinski JA. Encapsulation of bilayer vesicles by self-assembly. Nature. 1997;387(6628):61–4.
32. Edwards DA, Schneck F, Zhang I, Davis AMJ, Chen H, Langer R. Spontaneous vesicle formation at lipid bilayer membranes. Biophys J. 1996;71(3):1208–14.
33. Deville S, Berckmans P, Van Hoof R, Lambrichts I, Salvati A, Nelissen I. Comparison of extracellular vesicle isolation and storage methods using high-sensitivity flow cytometry. PLoS One. 2021;16(2):e0245835.
34. Torres Crigna A, Fricke F, Nitschke K, Worst T, Erb U, Karremann M, et al. Inter-Laboratory Comparison of Extracellular Vesicle Isolation Based on Ultracentrifugation. Transfus Med Hemother. 2021;48(1):48–59. Available from: http://www.ncbi.nlm.nih.gov/pubmed/33708052. Cited 2025 Jan 17.
35. Zonneveld MI, Brisson AR, van Herwijnen MJC, Tan S, van de Lest CHA, Redegeld FA, et al. Recovery of extracellular vesicles from human breast milk is influenced by sample collection and vesicle isolation procedures. J Extracell vesicles. 2014;3(1). Available from: http://www.ncbi.nlm.nih.gov/pubmed/25206958. Cited 2025 Jan 17.
36. Kalra H, Adda CG, Liem M, Ang CS, Mechler A, Simpson RJ, et al. Comparative proteomics evaluation of plasma exosome isolation techniques and assessment of the stability of exosomes in normal human blood plasma. Proteomics. 2013;13(22):3354–64.
37. Athman JJ, Sande OJ, Groft SG, Reba SM, Nagy N, Wearsch PA, et al. Mycobacterium tuberculosis membrane vesicles inhibit T Cell activation. J Immunol. 2017;198(5):2028–37.
38. Gupta S, Rodriguez GM. Isolation and characterization of extracellular vesicles produced by iron-limited mycobacteria. J Vis Exp. 2019;2019(152):e60359.
39. Rath P, Huang C, Wang T, Wang T, Li H, Prados-Rosales R, et al. Genetic regulation of vesiculogenesis and immunomodulation in Mycobacterium tuberculosis. Proc Natl Acad Sci U S A. 2013;110(49):E4790.
40. Prados-Rosales R, Carreño LJ, Batista-Gonzalez A, Baena A, Venkataswamy MM, Xu J, et al. Mycobacterial membrane vesicles administered systemically in mice induce a protective immune response to surface compartments of mycobacterium tuberculosis. mBio. 2014;5(5):10.
41. Prados-Rosales R, Brown L, Casadevall A, Montalvo-Quirós S, Luque-Garcia JL. Isolation and identification of membrane vesicle-associated proteins in Gram-positive bacteria and mycobacteria. MethodsX. 2014;1:124–9.

Available from: http://www.ncbi.nlm.nih.gov/pubmed/26150943. Cited 2025 Jan 17.
42. Lee J, Kim SH, Choi DS, Lee JS, Kim DK, Go G, et al. Proteomic analysis of extracellular vesicles derived from Mycobacterium tuberculosis. Proteomics. 2015;15(19):3331–7.
43. Ziegenbalg A, Prados-Rosales R, Jenny-Avital ER, Kim RS, Casadevall A, Achkar JM. Immunogenicity of mycobacterial vesicles in humans: identification of a new tuberculosis antibody biomarker. Tuberculosis. 2013;93(4):448–55.
44. White DW, Elliott SR, Odean E, Bemis LT, Tischler AD. Mycobacterium tuberculosis Pst/SenX3-RegX3 regulates membrane vesicle production independently of ESX-5 activity. mBio. 2018;9(3):10.
45. Kumar S, Mittal E, Deore S, Kumar A, Rahman A, Krishnasastry M V. Mycobacterial tlyA gene product is localized to the cell-wall without signal sequence. Front Cell Infect Microbiol. 2015;5:60. https://doi.org/10.3389/fcimb.2015.00060.
46. Jurkoshek KS, Wang Y, Athman JJ, Barton MR, Wearsch PA. Interspecies Communication between Pathogens and Immune Cells via Bacterial Membrane Vesicles. Front cell Dev Biol. 2016;4(NOV):125. Available from: http://www.ncbi.nlm.nih.gov/pubmed/27891500. Cited 2025 Jan 17.
47. Lucas M, Ryan JM, Watkins J, Early K, Kruh-Garcia NA, Mehaffy C, et al. Extraction and separation of mycobacterial proteins. Methods Mol Biol. 2021;2314:77–107.
48. Benedikter BJ, Bouwman FG, Vajen T, Heinzmann ACA, Grauls G, Mariman EC, et al. Ultrafiltration combined with size exclusion chromatography efficiently isolates extracellular vesicles from cell culture media for compositional and functional studies. Sci Rep. 2017;7(1):15297.
49. Wallace E, Hendrickson D, Tolli N, Mehaffy C, Peña M, Nick JA, et al. Culturing mycobacteria. Methods Mol Biol. 2021;2314:1–58.
50. Takayama K, Schnoes HK, Armstrong EL, Boyle RW. Site of inhibitory action of isoniazid in the synthesis of mycolic acids in Mycobacterium tuberculosis. J Lipid Res. 1975;16(4):308–17. Available from: https://pubmed.ncbi.nlm.nih.gov/806645/. Cited 2025 Jan 16.
51. Sartain MJ, Belisle JT. N-Terminal clustering of the O-glycosylation sites in the Mycobacterium tuberculosis lipoprotein SodC. Glycobiology. 2009;19(1):38–51.
52. Schneider CA, Rasband WS, Eliceiri KW. NIH Image to ImageJ: 25 years of image analysis. Nat Methods 2012 97. 2012 Jun;9(7):671–5. Available from: https://www.nature.com/articles/nmeth.2089. Cited 2025 Jan 17.
53. Kong AT, Leprevost FV, Avtonomov DM, Mellacheruvu D, Nesvizhskii AI. MSFragger: Ultrafast and comprehensive peptide identification in mass spectrometry-based proteomics. Nat Methods. 2017;14(5):513–20.
54. Yu F, Teo GC, Kong AT, Haynes SE, Avtonomov DM, Geiszler DJ, et al. Identification of modified peptides using localization-aware open search. Nat Commun. 2020;11(1):4065.
55. Yu F, Haynes SE, Teo GC, Avtonomov DM, Polasky DA, Nesvizhskii AI. Fast quantitative analysis of timsTOF PASEF data with MSFragger and IonQuant. Mol Cell Proteomics. 2020;19(9):1575–85.
56. Teo GC, Polasky DA, Yu F, Nesvizhskii AI. Fast deisotoping algorithm and its implementation in the MSFragger search engine. J Proteome Res. 2021;20(1):498–505.
57. Yu F, Haynes SE, Nesvizhskii AI. IonQuant enables accurate and sensitive label-free quantification with FDR-controlled match-between-runs. Mol Cell Proteomics. 2021;20:100077.
58. da Veiga LF, Haynes SE, Avtonomov DM, Chang HY, Shanmugam AK, Mellacheruvu D, et al. Philosopher: a versatile toolkit for shotgun proteomics data analysis. Nat Methods. 2020;17(9):869–70.
59. Yang KL, Yu F, Teo GC, Li K, Demichev V, Ralser M, et al. MSBooster: improving peptide identification rates using deep learning-based features. Nat Commun. 2023;14(1):4539.
60. R: The R Project for Statistical Computing. Available from: https://www.r-project.org/. Cited 2025 Jan 17.
61. CRAN: Package ggpubr. Available from: https://cran.r-project.org/web/packages/ggpubr/index.html. Cited 2025 Jan 17.
62. Pinheiro J, Bates D. Linear and Nonlinear Mixed Effects Models [R package nlme version 3.1–166]. CRAN Contrib Packag. 2024. Available from: https://cran.r-project.org/package=nlme. Cited 2025 Jan 17.
63. knitr - Elegant, flexible, and fast dynamic report generation with R - Yihui Xie | 谢益辉. Available from: https://yihui.org/knitr/. Cited 2025 Jan 17.
64. Wickham H, Averick M, Bryan J, Chang W, D'L, Mcgowan A, et al. Welcome to the Tidyverse. J Open Source Softw. 2019;4(43):1686. Available from: https://joss.theoj.org/papers/10.21105/joss.01686. Cited 2025 Jan 17.
65. Williams WR, Kendall LV. Blood collection in the guinea pig (Cavia porcellus). Lab Anim (NY). 2015;44(6):207–8.
66. R Companion 3E. Available from: https://www.john-fox.ca/Companion/downloads.html. Cited 2025 Jan 17.
67. Bates D, Mächler M, Bolker BM, Walker SC. Fitting Linear Mixed-Effects Models Using lme4. J Stat Softw. 2015;67(1):1–48. Available from: https://www.jstatsoft.org/index.php/jss/article/view/v067i01. Cited 2025 Jan 17.
68. Ahlmann-Eltze C, Patil I. ggsignif: R Package for Displaying Significance Brackets for "ggplot2." 2021 . Available from: https://osf.io/7awm6. Cited 2025 Jan 17.
69. CRAN: Package broom.mixed. Available from: https://cran.r-project.org/web/packages/broom.mixed/index.html. Cited 2025 Jan 17.
70. CRAN: Package dplyr. Available from: https://cran.r-project.org/web/packages/dplyr/index.html.
71. CRAN: Package GGally. Available from: https://cran.r-project.org/web/packages/GGally/index.html. Cited 2025 Jan 17.
72. Kassambara A. Pipe-Friendly Framework for Basic Statistical Tests [R package rstatix version 0.7.2]. CRAN Contrib Packag. 2023. Available from: https://cran.r-project.org/package=rstatix. Cited 2025 Jan 17.
73. Ogle DH, Doll JC, Wheeler AP, Dinno A. Simple Fisheries Stock Assessment Methods [R package FSA version 0.9.6]. CRAN Contrib Packag. 2025. Available from: https://cran.r-project.org/package=FSA. Cited 2025 Jan 17.
74. Kassambara A. "ggplot2" Based Publication Ready Plots [R package ggpubr version 0.6.0]. CRAN Contrib Packag. 2023. Available from: https://cran.r-project.org/package=ggpubr. Cited 2025 Jan 17.
75. Robinson D, Hayes A, Couch S. Convert Statistical Objects into Tidy Tibbles [R package broom version 1.0.7]. CRAN Contrib Packag. 2024 . Available from: https://cran.r-project.org/package=broom. Cited 2025 Jan 17.
76. Schloerke B, Cook D, Larmarange J, Briatte F, Marbach M, Thoen E, et al. Extension to "ggplot2" [R package GGally version 2.2.1]. CRAN Contrib Packag. 2024. Available from: https://cran.r-project.org/package=GGally. Cited 2025 Jan 17.
77. Cox J, Hein MY, Luber CA, Paron I, Nagaraj N, Mann M. Accurate proteome-wide label-free quantification by delayed normalization and maximal peptide ratio extraction, termed MaxLFQ. Mol Cell Proteomics. 2014;13(9):2513–26.
78. Kapopoulou A, Lew JM, Cole ST. The MycoBrowser portal: a comprehensive and manually annotated resource for mycobacterial genomes. Tuberculosis. 2011;91(1):8–13.
79. Schirmer S, Rauh L, Alebouyeh S, Delgado-Velandia M, Salgueiro VC, Lerma L, et al. Immunogenicity of Mycobacterial Extracellular Vesicles Isolated From Host-Related Conditions Informs About Tuberculosis Disease Status. Front Microbiol. 2022;13:907296. Available from: http://www.ncbi.nlm.nih.gov/pubmed/35814710. Cited 2025 Jan 17.
80. Rezwan M, Grau T, Tschumi A, Sander P. Lipoprotein synthesis in mycobacteria. Microbiology. 2007;153(3):652–8.
81. Raze D, Verwaerde C, Deloison G, Werkmeister E, Coupin B, Loyens M, et al. Heparin-Binding Hemagglutinin Adhesin (HBHA) Is Involved in Intracytosolic Lipid Inclusions Formation in Mycobacteria. Front Microbiol. 2018;9(SEP):2258. Available from: http://www.ncbi.nlm.nih.gov/pubmed/30333800. Cited 2025 Jan 17.
82. Li Y, Qian Y, Wang N, Qiu D, Cao H, Wang Y, et al. The functions and applications of extracellular vesicles derived from Mycobacterium tuberculosis. Biomed Pharmacother. 2023;168:115767.
83. de Souza GA, Leversen NA, Målen H, Wiker HG. Bacterial proteins with cleaved or uncleaved signal peptides of the general secretory pathway. J Proteomics. 2011;75(2):502–10.
84. Xiong Y, Chalmers MJ, Gao FP, Cross TA, Marshall AG. Identification of Mycobacterium tuberculosis H37Rv integral membrane proteins by one-dimensional gel electrophoresis and liquid chromatography electrospray ionization tandem mass spectrometry. J Proteome Res. 2005;4(3):855–61.
85. Shahbaaz M, Potemkin V, Bisetty K, Hassan MI, Hussien MA. Classification and functional analyses of putative virulence factors of Mycobacterium tuberculosis: a combined sequence and structure based study. Comput Biol Chem. 2020;87:107270.

86. Perez-Riverol Y, Bai J, Bandla C, García-Seisdedos D, Hewapathirana S, Kamatchinathan S, et al. The PRIDE database resources in 2022: a hub for mass spectrometry-based proteomics evidences. Nucleic Acids Res. 2022;50(D1):D543–52.

Publisher's Note